

# Models for Velocity Decrease in HH34

Lorenzo Zaninetti

Physics Department, via P.Giuria 1, Turin, Italy

Email: zaninetti@ph.unito.it

**How to cite this paper:** Zaninetti, L. (2019) Models for Velocity Decrease in HH34. *International Journal of Astronomy and Astrophysics*, 9, 302-320.  
<https://doi.org/10.4236/ijaa.2019.93022>

**Received:** July 24, 2019

**Accepted:** September 16, 2019

**Published:** September 19, 2019

Copyright © 2019 by author(s) and Scientific Research Publishing Inc. This work is licensed under the Creative Commons Attribution International License (CC BY 4.0).

<http://creativecommons.org/licenses/by/4.0/>



Open Access

---

## Abstract

The conservation of the energy flux in turbulent jets that propagate in the interstellar medium (ISM) allows us to deduce the law of motion when an inverse power law decrease of density is considered. The back-reaction that is caused by the radiative losses for the trajectory is evaluated. The velocity dependence of the jet with time/space is applied to the jet of HH34, for which the astronomical data of velocity versus time/space are available. The introduction of precession and constant velocity for the central star allows us to build a curved trajectory for the superjet connected with HH34. The bow shock that is visible in the superjet is explained in the framework of the theory of the image in the case of an optically thin layer.

## Keywords

Herbig-Haro Objects, Bok Globules, Bipolar Outflows

---

## 1. Introduction

The equation of motion plays a relevant role in our understanding of the physics of the Herbig-Haro objects (HH) after [1] [2]. A common example is to evaluate the velocity of the jet in HH34 as 300 km/s, see [3], without paying attention to its spatial or temporal evolution. A precise evaluation of the evolution of the jet's velocity with time in HH34 has been done, for example, by [4]. It is, therefore, possible to speak of proper motions of young stellar outflows, see [5] [6] [7] [8].

The first set of theoretical efforts exclude the magnetic field: [9] have modeled the slowing down of the HH 34 superjet as a result of the jet's interaction with the surrounding environment, [10] have shown that a velocity profile in the jet beam is required to explain the observed acceleration in the position-velocity diagram of the HH jet, [11] found some constraints on the physical and chemical parameters of the clump ahead of HHs and [12] reviewed some important

understanding of outflows from young stars.

The second set of theoretical efforts include the magnetic field: [13] analysed the HH 1-2 region in the L1641 molecular cloud and found a straight magnetic field of about 130 micro-Gauss; [14] analysed HH 211 and found field lines of the magnetic field with different orientations; [15] analysed HH 111 and found evidence for magnetic braking.

These theoretical efforts to understand HH objects leave a series of questions unanswered or partially answered, as follows:

- Is it possible to find a law of motion for turbulent jets in the presence of a medium with a density that decreases as a power law?
- Is it possible to introduce the back reaction into the equation of motion for turbulent jets to model the radiative losses?
- Can we model the bending of the super-jet connected with HH34?
- Can we explain the bow shock visible in HH34 with the theory of the image?

To answer these questions, this paper reviews in Section 2 the velocity observations of HH34 at a 9 yr time interval, Section 3 analyses two simple models as given by the Stoke's and Newton's laws of resistance, Section 4 applies the conservation of the energy flux in a turbulent jet to find an equation of motion, Section 5 models the extended region of HH34, the so called "superjet", and Section 6 reports some analytical and numerical algorithms that allow us to build the image of HH34.

## 2. Preliminaries

The velocity evolution of the HH34 jet has recently been analysed in [SII] 2, (672 nm), frames and **Table 1** in [4] reports the Cartesian coordinates, the velocities, and the dynamical time for 18 knots in 9 years of observations. To start with time,  $t$ , equal to zero, we fitted the velocity versus distance with the following power law

$$v(x; x_0, v_0) = v_0 \times (x/x_0)^\alpha, \quad (1)$$

where  $v$  and  $x$  are the velocity and the length of the jet,  $v_0$  is the velocity at  $x = x_0$  and  $\alpha$  with its relative error is a parameter to be found with a fitting procedure. The integration of this equation gives the time as a function of the position,  $x$ , as given by the fit

$$t = -\frac{x^{-\alpha+1}x_0^\alpha - x_0}{(\alpha-1)v_0}, \quad (2)$$

where  $x_0$  is the position at  $t = 0$ . The fitted trajectory, distance versus time, is

$$x(t; x_0, v_0) = e^{\frac{\alpha \ln(x_0) - \ln(-t(\alpha-1)v_0 + x_0)}{\alpha-1}}, \quad (3)$$

and the fitted velocity as function of time is

$$v(t; x_0, v_0) = v_0 \left( \frac{1}{x_0} e^{\frac{\alpha \ln(x_0) - \ln(-t(\alpha-1)v_0 + x_0)}{\alpha-1}} \right)^\alpha. \quad (4)$$

**Table 1.** Numerical values for the physical parameters of HH34.

Knot	$x$ (pc)	$v$ (km/s)	Time (yr)
1	0.002594	171.01	0.
2	0.004021	202.15	7.484
3	0.007214	171.23	25.131
4	0.009434	176.13	37.903
5	0.012545	164.04	56.303
6	0.016017	163.24	77.381
7	0.018125	141.03	90.415
8	0.019580	162.00	99.502
9	0.021046	165.07	108.71
10	0.02622	156.08	141.76
11	0.02745	156.08	149.75
12	0.03096	142.03	172.63
13	0.03528	148.03	201.20
14	0.03723	148.03	214.17
15	0.04050	148.569855	236.15
16	0.04420	138.293167	261.17
17	0.04880	134.082062	292.60
18	0.05684	143.003494	348.25

The adopted physical units are pc for length and year for time, and the useful conversion for the velocity is  $1 \text{ pc/year} = 979682.5397 \text{ km/s}$ .

The fit of Equation (1) when  $x$  is expressed in pc gives

$$v(x) = 0.000107x^{-0.0998 \pm 0.01618} \text{ pc/yr}, \quad (5)$$

from which we can conclude that the velocity decreases with increasing distance, see **Figure 1**.

The time is derived from Equation (2) and **Table 1** reports the basic parameters of HH34. This time is more continuous in respect to the dynamical time reported in column 6 of **Table 1** in [4].

### 3. Two Simple Models

When a jet moves through the interstellar medium (ISM), a retarding drag force  $F_{drag}$ , is applied. If  $v$  is the instantaneous velocity, then the simplest model assumes

$$F_{drag} \propto v^n, \quad (6)$$

where  $n$  is an integer. Here, the case of  $n=1$  and  $n=2$  is considered. In classical mechanics,  $n=1$  is referred to as Stoke's law of resistance and  $n=2$  is referred to as Newton's law of resistance.

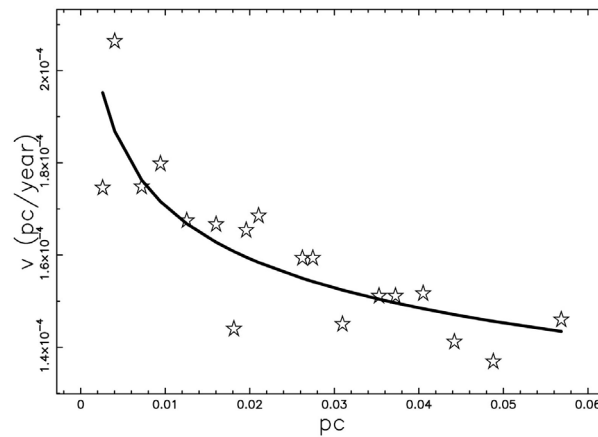


**Figure 1.** Observational points of velocity in pc/yr versus distance in pc (empty circles) and best fit as given by Equation (1) (full line).

### 3.1. Stoke's Behaviour

The equation of motion is given by

$$\frac{dv(t)}{dt} = -Bv(t). \quad (7)$$

The velocity as function of time is

$$v = v_0 e^{-Bt}, \quad (8)$$

where  $v_0$  is the initial velocity. The distance at time  $t$  is

$$x = s(t) = x_0 - \frac{v_0 e^{-Bt}}{B} + \frac{v_0}{B}. \quad (9)$$

The time as function of distance is obtained by the inversion of this equation

$$t = \frac{1}{B} - \ln \left( -\frac{xB - Bx_0 - v_0}{v_0} \right). \quad (10)$$

The velocity as a function of space is

$$v(x; x_0, v_0, B) = -xB + Bx_0 + v_0. \quad (11)$$

The numerical value of  $B$  is

$$B = -\frac{v_0 - v_1}{x_0 - x_1}, \quad (12)$$

where  $v_1$  is the velocity at point  $x_1$ ; the data of **Table 1** gives  $B = 0.0009549$  (**Figure 2**).

### 3.2. Newton's Behaviour

The equation of motion is

$$\frac{dv(t)}{dt} = -Av(t)^2. \quad (13)$$

The velocity as function of time is

$$v = v(t) = \frac{v_0}{Atv_0 + 1}, \quad (14)$$

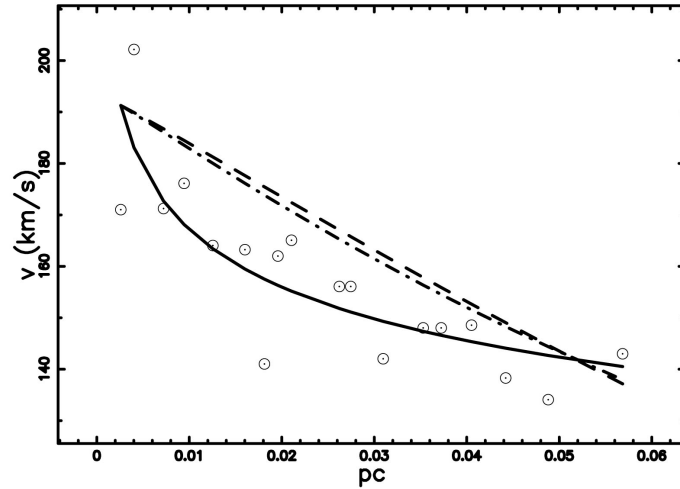


**Figure 2.** Observational points of velocity in pc/yr versus distance in pc (empty circles), best fit as given by Equation (1) (full line), Stokes behaviour as given by Equation (11) (dashed line) and Newton behaviour as given by Equation (17) (dot-dash-dot-dash).

where  $v_0$  is the initial velocity. The distance at time  $t$  is

$$x = s(t) = \frac{\ln(Atv_0 + 1)}{A} + x_0. \tag{15}$$

The time as function of distance is obtained by the inversion of the above equation

$$t = \frac{e^{xA - Ax_0} - 1}{Av_0}. \tag{16}$$

The velocity as function of the distance is

$$v(x; x_0, v_0, A) = \frac{v_0}{e^{xA - Ax_0}}. \tag{17}$$

The numerical value of  $A$  is

$$A = -\frac{1}{x_0 - x_1} \ln\left(\frac{v_0}{v_1}\right), \tag{18}$$

where  $v_1$  is the velocity at point  $x_1$ ; the data of **Table 1** gives  $A = 5.68381834$ .

#### 4. Energy Flux Conservation

The conservation of the energy flux in a turbulent jet requires a perpendicular section to the motion along the Cartesian  $x$ -axis,  $A$

$$A(r) = \pi r^2 \tag{19}$$

where  $r$  is the radius of the jet. Section  $A$  at position  $x_0$  is

$$A(x_0) = \pi \left( x_0 \tan\left(\frac{\alpha}{2}\right) \right)^2 \tag{20}$$

where  $\alpha$  is the opening angle and  $x_0$  is the initial position on the  $x$ -axis. At position  $x$ , we have

$$A(x) = \pi \left( x \tan\left(\frac{\alpha}{2}\right) \right)^2. \quad (21)$$

The conservation of energy flux states that

$$\frac{1}{2} \rho(x_0) v_0^3 A(x_0) = \frac{1}{2} \rho(x) v(x)^3 A(x) [B \quad (22)$$

where  $v(x)$  is the velocity at position  $x$  and  $v_0(x_0)$  is the velocity at position  $x_0$ , see Formula A28 in [16]. More details can be found in [17] [18]. The density is assumed to decrease as a power law

$$\rho = \rho_0 \left( \frac{x_0}{x} \right)^\delta \quad (23)$$

where  $\rho_0$  is the density at  $x = x_0$  and  $\delta$  a positive parameter. The differential equation that models the energy flux is

$$\frac{1}{2} \left( \frac{x_0}{x} \right)^\delta \left( \frac{d}{dt} x(t) \right)^3 x^2 - \frac{1}{2} v_0^3 x_0^2 = 0. \quad (24)$$

The velocity as a function of the position,  $x$ ,

$$v(x) = \frac{\sqrt[3]{x_0^2 \left( \left( \frac{x_0}{x} \right)^\delta \right)^2} x v_0}{\left( \frac{x_0}{x} \right)^\delta x}. \quad (25)$$

**Figure 3** reports the velocity as a function of the distance and the observed points.

We now have four models for the velocity as a function of time and **Table 2** reports the merit function  $\chi^2$ , which is evaluated as

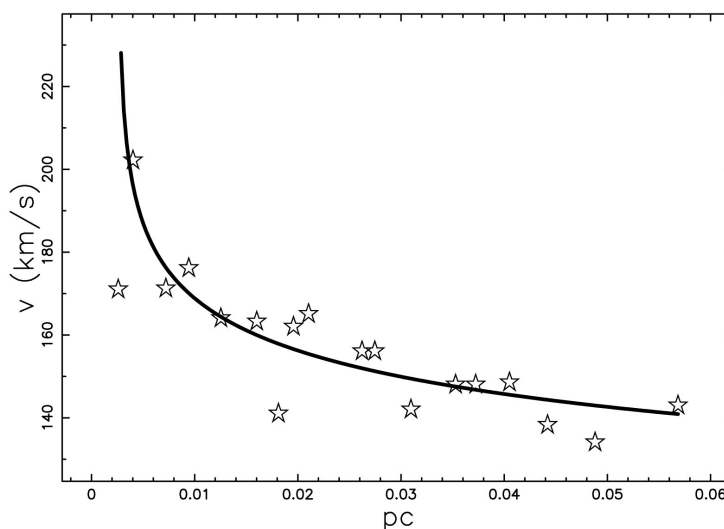


**Figure 3.** Observational points of velocity in pc/yr versus distance in pc (empty stars). The theoretical fit is given by Equation (25) (full line) with parameters  $x_0 = 0.00259$  pc,  $v_0 = 191.27$  km/s and  $\delta = 1.7$ .

**Table 2.** The values of the  $\chi^2$  for four models of velocity of HH34.

Model	$\chi^2$
Power law fit (no physics)	1479
Stoke's behaviour	3813
Newton's behaviour	3317
Turbulent jet	2373

$$\chi^2 = \sum_{i=1}^N [y_{i,theo} - y_{i,obs}]^2 \tag{26}$$

where  $y_{i,obs}$  represents the observed value at position  $i$  and  $y_{i,theo}$  the theoretical value at position  $i$ . A careful analysis of **Table 2** allows us to conclude that the turbulent jet performs better in respect to the Stokes's and Newton's behavior.

The trajectory, *i.e.* the distance as function of the time,

$$x(t; r_0, v_0, \delta) = x_0 e^{\frac{1}{\delta-5} \left( 3 \ln(3) - 3 \ln(5-\delta) - \ln \left( \frac{t^3 v_0^3}{x_0^3} \right) \right)} \tag{27}$$

and the velocity as function of time

$$v(t; r_0, v_0, \delta) = \frac{1}{x_0} 3^{\frac{-2\delta+1}{\delta-5}} (5-\delta)^{\frac{2\delta-1}{\delta-5}} \sqrt[3]{x_0^3 \left( \left( \frac{t^3 v_0^3}{x_0^3} \right)^{(\delta-5)^{-1}} \right)^{2\delta} \left( \frac{t^3 v_0^3}{x_0^3} \right)^{-(\delta-5)^{-1}}} \times v_0 \left( e^{\frac{1}{\delta-5} \left( -3 \ln(3) + 3 \ln(5-\delta) + \ln \left( \frac{t^3 v_0^3}{x_0^3} \right) \right)} \right)^{-\delta} e^{\frac{1}{\delta-5} \left( -3 \ln(3) + 3 \ln(5-\delta) + \ln \left( \frac{t^3 v_0^3}{x_0^3} \right) \right)} \tag{28}$$

**Figure 4** reports the trajectory as a function of time and of the observed points.

The rate of mass flow at the point  $x$ ,  $\dot{m}(x)$ , is

$$\dot{m}(x; v, \alpha) = \rho v(x) \pi \left( x \tan \left( \frac{\alpha}{2} \right) \right)^2 \tag{29}$$

and the astrophysical version is

$$\begin{aligned} \dot{m}(x; x_0, v_{0,km/s}, M_{\odot}, \alpha) \\ = 7.9252910^{-8} n x^{4/3-2/3\delta} (\tan(\alpha/2))^2 x_0^{2/3+2/3\delta} v_{0,km/s} M_{\odot}/yr \end{aligned} \tag{30}$$

where  $\alpha$  is the opening angle in rad,  $x$  and  $x_0$  are expressed in pc,  $n$  is the number density of protons at  $x = x_0$  expressed in particles  $\text{cm}^{-3}$ ,  $M_{\odot}$  is the solar mass and  $v_{0,km/s}$  is the initial velocity at point  $x_0$  expressed in km/s. This rate of mass flow as function of the distance  $x$  increases when  $\delta < 2$ , is constant when  $\delta = 2$ , and decreases when  $\delta > 2$ .

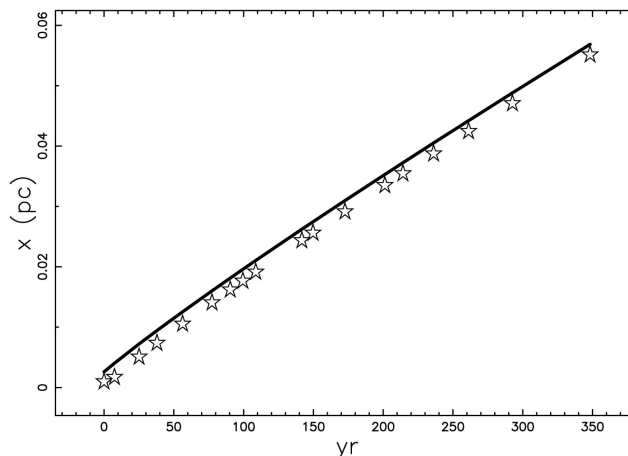


**Figure 4.** Observational points of distance in pc versus time in years (empty stars). The theoretical curve is given by Equation (27) (full line) with the same parameters as in Figure 3.

### The Back Reaction

Let us suppose that the radiative losses are proportional to the flux of energy

$$-\epsilon \frac{1}{2} \rho(x) v(x)^3 A(x), \quad (31)$$

where  $\epsilon$  is a constant that is thought to be  $\ll 1$ . By inserting in the above equation the considered area,  $A(x)$ , and the power law density here adopted the radiative losses are

$$-\epsilon \frac{1}{2} \rho_0 \left( \frac{x_0}{x} \right)^\delta v^3 \pi x^2 \left( \tan \left( \frac{\alpha}{2} \right) \right)^2. \quad (32)$$

By inserting in this equation the velocity to first order as given by Equation (25), the radiative losses,  $Q(x; x_0, v_0, \delta, \epsilon)$ , are

$$Q(x; x_0, v_0, \delta, \epsilon) = -\epsilon \frac{1}{2} \rho_0 v_0^3 \pi x_0^2 \left( \tan \left( \frac{\alpha}{2} \right) \right)^2 x, \quad (33)$$

The sum of the radiative losses between  $x_0$  and  $x$  is given by the following integral,  $L$ ,

$$\begin{aligned} L(x; x_0, v_0, \delta, \epsilon) &= \int_{x_0}^x Q(x; x_0, v_0, \delta, \epsilon) dx \\ &= -\epsilon \frac{1}{2} \rho_0 v_0^3 \pi x_0^2 \left( \tan \left( \frac{\alpha}{2} \right) \right)^2 (x - x_0). \end{aligned} \quad (34)$$

The conservation of the flux of energy in the presence of the back-reaction due to the radiative losses is

$$\frac{1}{2} \left( v_0^3 x_0^2 \epsilon x - v_0^3 x_0^3 \epsilon + \left( \frac{x_0}{x} \right)^\delta v^3 x^2 \right) \rho_0 = \frac{1}{2} \rho_0 v_0^3 x_0^2 \quad (35)$$

The real solution of the cubic equation for the velocity to the second order,  $v_c(x; \delta, x_0, v_0)$ , is

$$v_c(x; \delta, x_0, v_0) = \sqrt[3]{-(\epsilon x - \epsilon x_0 - 1) x_0^{2+2\delta} x^{4-2\delta} v_0 x^{-2+\delta} x_0^{-\delta}}. \quad (36)$$



**Figure 5** reports the effect of introducing the losses on the velocity as function of the distance for a given value of  $\epsilon$ , *i.e.* the velocity decreases more quickly.

The presence of the back-reaction allows us to evaluate the jet's length, which can be derived from the minimum in the corrected velocity to second order as a function of  $x$ ,

$$\frac{\partial v_\epsilon(x; \delta, x_0, v_0)}{\partial x} = 0, \tag{37}$$

which is

$$\frac{-v_0 (\delta \epsilon x - \delta \epsilon x_0 - \epsilon x + 2 \epsilon x_0 - \delta + 2) x_0^{-\delta/3+2/3} x^{-5/3+\delta/3}}{3(1+\epsilon(x-x_0))^{2/3}} = 0. \tag{38}$$

The solution for  $x$  of the above minimum allows us to derive the jet's length,  $x_j$ ,

$$x_j = \frac{\delta \epsilon x_0 - 2 \epsilon x_0 + \delta - 2}{\epsilon(\delta - 1)}. \tag{39}$$

**Figure 6** reports an example of the jet's length as a function of the parameter  $\delta$ .

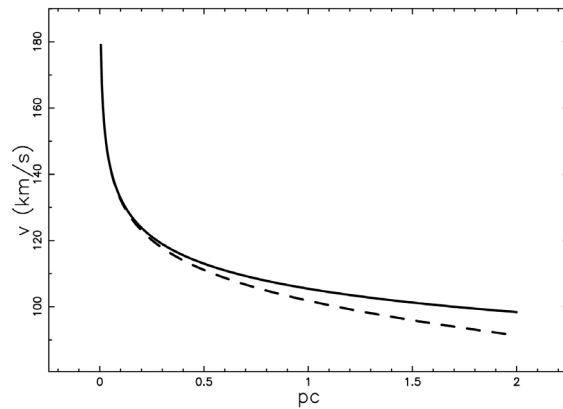


**Figure 5.** Velocity to the second order as function of the distance, see Equation (36), when  $\epsilon = 0$  (full line) and  $\epsilon = 0.1$  (dashed line), other parameters as in **Figure 3**.

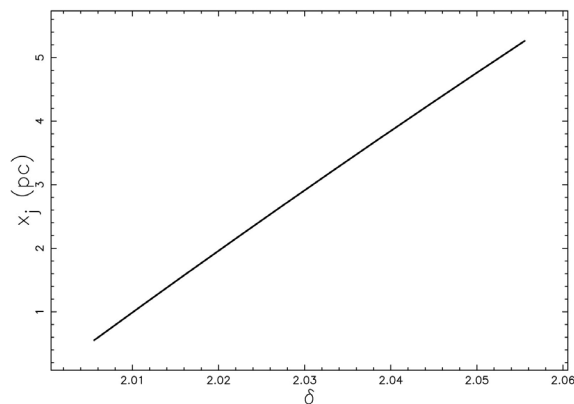


**Figure 6.** Length of the jet as a function of  $\delta$ , and the other parameters are as in **Figure 3**.

## 5. The Extended Region

To deal with the complex shape of the continuation of HH34 (e.g. see the new region HH173 discovered by [19]), we should include the precession of the source and motion of the host star, following a scheme outlined in [20]. The various coordinate systems are  $\mathbf{x} = (x, y, z)$ ,  $\mathbf{x}^{(1)} = (x^{(1)}, y^{(1)}, z^{(1)})$ , ...,  $\mathbf{x}^{(3)} = (x^{(3)}, y^{(3)}, z^{(3)})$ . The vector representing the motion of the jet is represented by the following  $1 \times 3$  matrix:

$$G = \begin{bmatrix} x(t) \\ 0 \\ 0 \end{bmatrix}, \quad (40)$$

where the jet motion  $L(t)$  is considered along  $x$  axis.

The jet axis,  $x$ , is inclined at an angle  $\Psi_{prec}$  relative to an axis  $x^{(1)}$ , and therefore the  $3 \times 3$  matrix, which represents a rotation through  $z$  axis, is given by:

$$F = \begin{bmatrix} \cos(\Psi_{prec}) & -\sin(\Psi_{prec}) & 0 \\ \sin(\Psi_{prec}) & \cos(\Psi_{prec}) & 0 \\ 0 & 0 & 1 \end{bmatrix}. \quad (41)$$

The jet is undergoing precession around the  $x^{(1)}$  axis and  $\Omega_{prec}$  is the angular velocity of precession expressed in radians per unit time. The transformation from the coordinates  $x^{(1)}$  fixed in the frame of the precessing jet to the nonprecessing coordinate  $\mathbf{x}^{(2)}$  is represented by the  $3 \times 3$  matrix

$$P = \begin{bmatrix} 1 & 0 & 0 \\ 0 & \cos(\Omega_{prec}t) & -\sin(\Omega_{prec}t) \\ 0 & \sin(\Omega_{prec}t) & \cos(\Omega_{prec}t) \end{bmatrix}. \quad (42)$$

The last translation represents the change of the framework from  $(\mathbf{x}^{(2)})$ , which is co-moving with the host star, to a system  $(\mathbf{x}^{(3)})$ , in comparison to which the host star is in a uniform motion. The relative motion of the origin of the coordinate system  $(x^{(3)}, y^{(3)}, z^{(3)})$  is defined by the Cartesian components of the star velocity  $v_x, v_y, v_z$ , and the required  $1 \times 3$  matrix transformation representing this translation is

$$B = \begin{bmatrix} v_x t \\ v_y t \\ v_z t \end{bmatrix}. \quad (43)$$

On assuming, for the sake of simplicity, that  $v_x = 0$  and  $v_z = 0$ , the translation matrix becomes

$$B = \begin{bmatrix} 0 \\ v_y t \\ 0 \end{bmatrix}. \quad (44)$$

The final  $1 \times 3$  matrix  $A$  representing the ‘‘motion law’’ can be found by

composing the four matrices already described;

$$A = B + (P \cdot F \cdot G) = \begin{bmatrix} \cos(\Psi_{prec})x(t) \\ v_y t + \cos(\Omega_{prec}t)\sin(\Psi_{prec})x(t) \\ \sin(\Omega_{prec}t)\sin(\Psi_{prec})x(t) \end{bmatrix}. \quad (45)$$

The three components of the previous  $1 \times 3$  matrix  $A$  represent the jet's motion along the Cartesian coordinates as given by an observer who sees the star moving in a uniform motion. The point of view of the observer can be modeled by introducing the matrix  $E$ , which represents the three Eulerian angles  $\Theta, \Phi, \Psi$ , see [21]. A typical trajectory is reported in **Figure 7** and a particularised point of view of the same trajectory is reported in **Figure 8** in which a loop is visible.

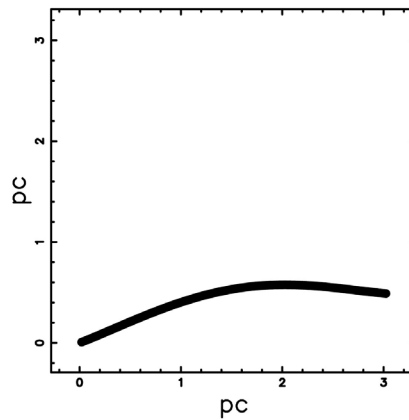


**Figure 7.** Continuous trajectory of the superjet connected with HH34: the three Eulerian angles characterising the point of view are  $\Phi = 0^\circ$ ,  $\Theta = 0^\circ$  and  $\Psi = 0^\circ$ . The precession is characterised by the angle  $\Psi_{prec} = 10^\circ$  and by the angular velocity

$\Omega_{prec} = 0.00496551674 [^\circ/\text{year}]$ . The star has velocity  $v_y = 31.107 \text{ km/s}$ , the considered time is 29,000 yr and the other parameters are as in **Figure 3**.

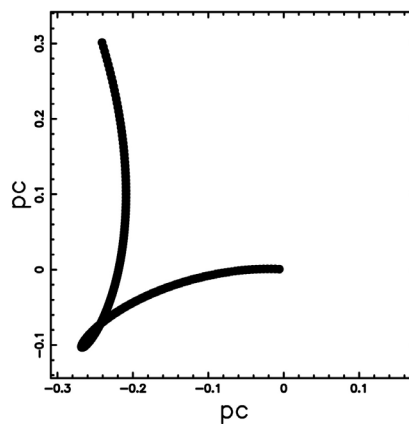


**Figure 8.** Continuous trajectory of the superjet connected with HH34: the three Eulerian angles characterising the point of view are  $\Phi = 100^\circ$ ,  $\Theta = 77^\circ$  and  $\Psi = 135^\circ$ . The other parameters as in **Figure 7**.

## 6. Image Theory

This section summarises the continuum observations of HH34, reviews the transfer equation with particular attention to the case of an optically thin layer, analyses a simple analytical model for theoretical intensity, reports the numerical algorithm that allows us to build a complex image and introduces the theoretical concept of emission from the knots.

### 6.1. Observations

The system of the jet and counter jet of HH34 has been analysed at 1.5  $\mu\text{m}$  and 4.5  $\mu\text{m}$ , see **Figure 3** in [3]. The intensity is almost constant,

$$I_{1.5} \approx 8 \times 10^{16} \text{ erg} \cdot \text{s}^{-1} \text{ arcsec}^{-2} \quad \text{for the first } 12'' \text{ of the jet and}$$

$I_{1.5} \approx 3 \times 10^{16} \text{ erg} \cdot \text{s}^{-1} \text{ arcsec}^{-2}$  for the first 20'' of the counter jet. At larger distances, the intensity drops monotonically. At a distance of 414 pc as given by [4] the conversion between physical and angular distance is  $1 \text{ pc} = 498.224''$ . For example, at 1.5  $\mu\text{m}$ , the emission is mainly due to the [Fe II] 1.64  $\mu\text{m}$  line.

### 6.2. The Transfer Equation

For the transfer equation in the presence of emission only see, for example, [22] or [23], is

$$\frac{dI_\nu}{ds} = -k_\nu \rho I_\nu + j_\nu \rho, \quad (46)$$

where  $I_\nu$  is the specific intensity,  $s$  is the line of sight,  $j_\nu$  is the emission coefficient,  $k_\nu$  is a mass absorption coefficient,  $\rho$  is the density of mass at position  $s$ , and the index  $\nu$  denotes the frequency of emission. The solution to Equation (46) is

$$I_\nu(\tau_\nu) = \frac{j_\nu}{k_\nu} (1 - e^{-\tau_\nu(s)}), \quad (47)$$

where  $\tau_\nu$  is the optical depth at frequency  $\nu$ :

$$d\tau_\nu = k_\nu \rho ds. \quad (48)$$

We now continue to analyse a case of an optically thin layer in which  $\tau_\nu$  is very small (or  $k_\nu$  is very small) and where the density  $\rho$  is replaced by the concentration  $C(s)$  of the emitting particles:

$$j_\nu \rho = KC(s), \quad (49)$$

where  $K$  is a constant. The intensity is now

$$I_\nu(s) = K \int_{s_0}^s C(s') ds' \quad \text{optically thin layer,} \quad (50)$$

which in the case of constant density,  $C$ , is

$$I_\nu(s) = KC \times (s - s_0) \quad \text{optically thin layer.} \quad (51)$$

The increase in brightness is proportional to the concentration of particles integrated along the line of sight.

### 6.3. Theoretical Intensity

The flux of observed radiation along the centre of the jet,  $I_c$  is assumed to scale as

$$I_c(x; x_0, v_0, b, \epsilon) \propto \frac{Q(x; x_0, v_0, b, \epsilon)}{x^2}, \tag{52}$$

where  $Q$ , the radiative losses, is given by Equation (33). The explicit form of this equation is

$$I_c(x; x_0, v_0, b, \epsilon) = -\frac{1}{2} \frac{(-1 + (x - x_0)\epsilon) x_0^2 v_0^3 \pi (\tan(\alpha/2))^2 \rho_0}{x^2}. \tag{53}$$

This relation connects the observed intensity of radiation with the rate of energy transfer per unit area. A typical example of the jet of HH34 at 4.5  $\mu\text{m}$  is reported in **Figure 9**.

### 6.4. Emission from a Cylinder

A thermal model for the image is characterised by a constant temperature and density in the internal region of the cylinder. Therefore, we assume that the number density  $C$  is constant in a cylinder of radius  $a$  and then falls to 0, see the simplified transfer Equation (51). The line of sight when the observer is situated at the infinity of the  $x$ -axis and the cylinder's axis is in the perpendicular position is the locus parallel to the  $x$ -axis, which crosses the position  $y$  in a Cartesian  $x$ - $y$  plane and terminates at the external circle of radius  $a$ . A similar treatment for the sphere is given in [24]. The length of this locus in the optically thin layer approximation is

$$l_{ab} = 2 \times (\sqrt{a^2 - y^2}); \quad 0 \leq y < a. \tag{54}$$

The number density  $C_m$  is constant in the circle of radius  $a$  and therefore the intensity of the radiation is

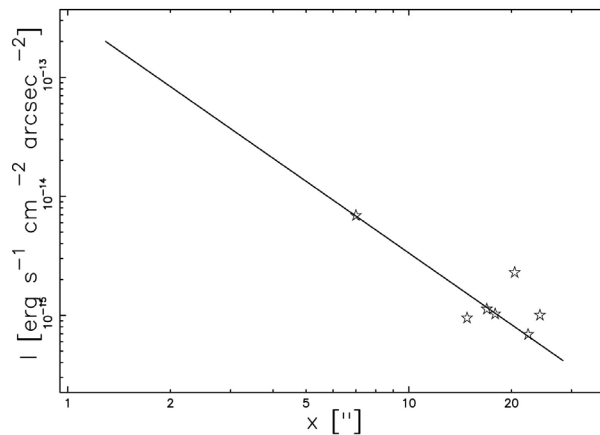


**Figure 9.** Observational points of intensity at 4.5  $\mu\text{m}$  (empty stars) and theoretical curve as given by Equation (53) (full line). when  $\epsilon = 1/100$ ,  $\rho_0 = 1$ ,  $\alpha = 2.86^\circ$  and other parameters as in **Figure 3**.

$$I_{0a} = C_m \times 2 \times (\sqrt{a^2 - y^2}); \quad 0 \leq y < a. \quad (55)$$

A typical example of this cut is reported in **Figure 10** and the intensity of all the cylinder is reported in **Figure 11**.

### 6.5. Numerical Image

The numerical algorithm that allows us to build a complex image in the optically thin layer approximation is now outlined.

- An empty, value = 0, memory grid  $\mathcal{M}(i, j, k)$  which contains  $400^3$  pixels is considered.
- The points which fill the jet in a uniform way to simulate the constant density in the emitting particles are inserted, value = 1, in  $\mathcal{M}(i, j, k)$
- Each point of  $\mathcal{M}(i, j, k)$  has spatial coordinates  $x, y, z$  which can be represented by the following  $1 \times 3$  matrix,  $A$ ,

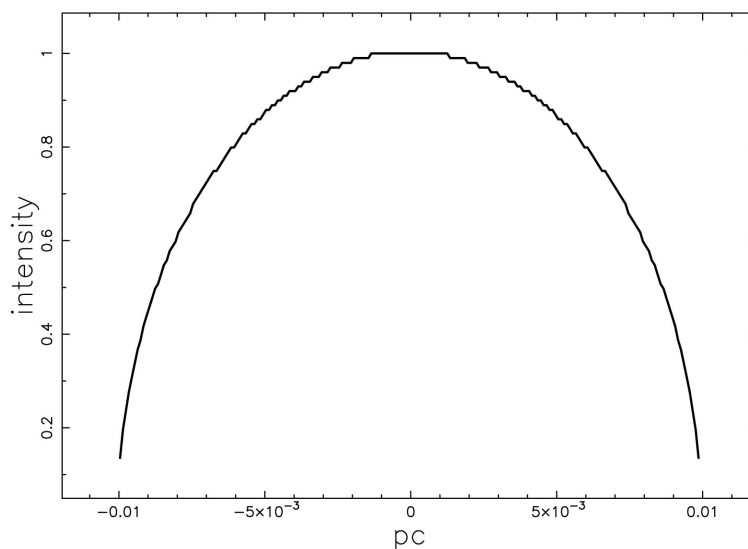


**Figure 10.** 1D cut of the intensity,  $I$ , when  $a = 0.01$  pc.

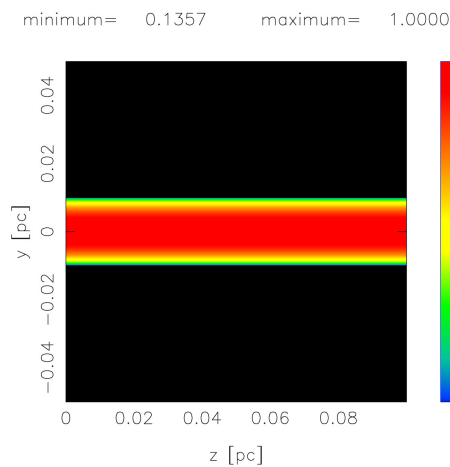


**Figure 11.** 2D map of the intensity of a jet which has length 0.1 pc and radius of 0.01 pc.

$$A = \begin{bmatrix} x \\ y \\ z \end{bmatrix}. \quad (56)$$

The orientation of the object is characterised by the Euler angles  $(\Phi, \Theta, \Psi)$  and therefore by a total  $3 \times 3$  rotation matrix,  $E$ , see [21]. The matrix point is represented by the following  $1 \times 3$  matrix,  $B$ ,

$$B = E \cdot A. \quad (57)$$

- The intensity 2D map is obtained by summing the points of the rotated images.

A typical result of the simulation is reported in **Figure 12**, which should be compared with the observed image as given by **Figure 13**.

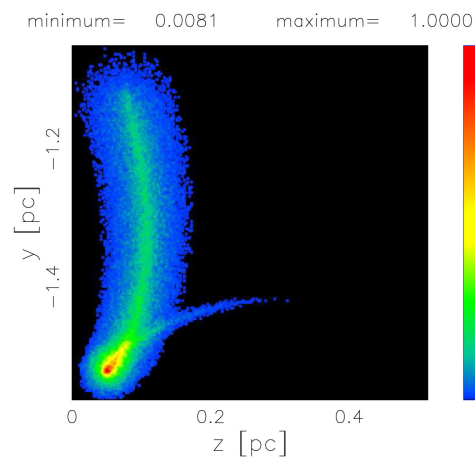


**Figure 12.** 2D intensity map of HH34, parameters as in **Figure 8**.

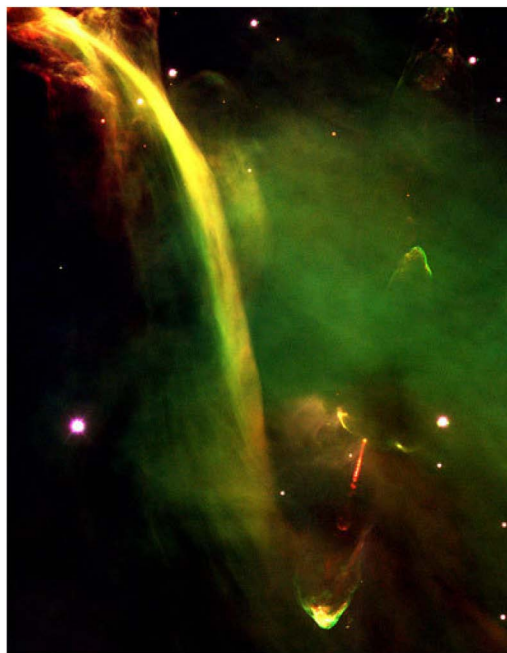


**Figure 13.** Three-color composite image of the young object HH34.

## 6.6. The Mathematical Knots

The trefoil knot is defined by the following parametric equations:

$$x = \sin(t) + 2\sin(2t) \quad (58)$$

$$y = \cos(t) - 2\cos(2t) \quad (59)$$

$$z = -\sin(3t) \quad (60)$$

with  $0 \leq t \leq 2\pi$ . The visual image depends on the Euler angles, see **Figure 14**.

The image in the optically thin layer approximation can be obtained by the numerical method developed in Section 6.5 and is reported in **Figure 15**.

This 2D map in the theoretical intensity of emission shows an enhancement where two mathematical knots apparently intersect.

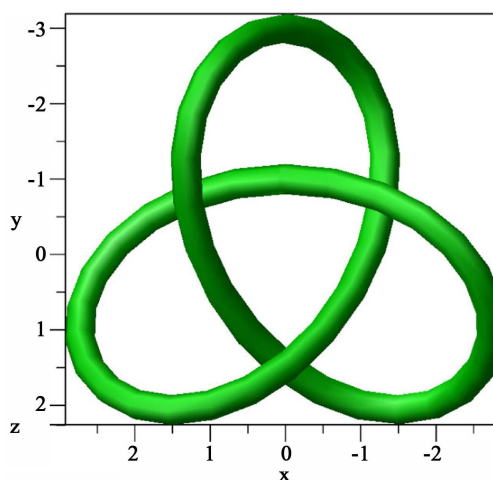


**Figure 14.** 3D view of the trefoil when the three Eulerian angles which characterise the point of view are  $\Phi = 0^\circ$ ,  $\Theta = 90^\circ$  and  $\Psi = 0^\circ$ .

minimum= 0.3182      maximum= 1.0000

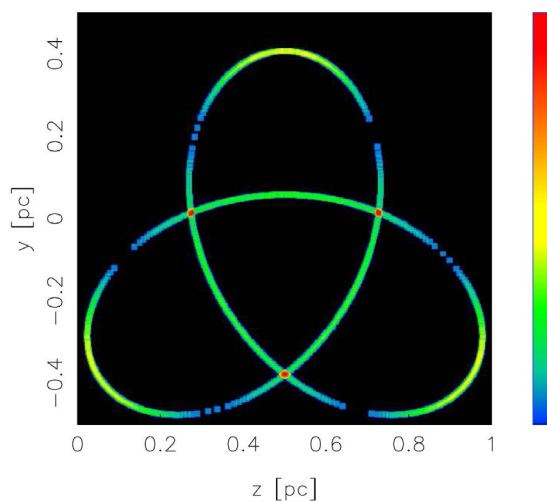


**Figure 15.** Image of the trefoil with parameters as in **Figure 14**, the side of the box in pc is 1 and the radius of the tube in pc is 0.006.



## 7. Conclusions

### Laws of motion:

We analysed two simple models for the law of motion in HH objects as given by the Stoke's and Newton's behaviour, see Section 3. A third law of motion is used for turbulent jets in the presence of a medium whose density decreases with a power law, as given by Equation (23). The model that is adopted for the turbulent jets conserves the flux of energy. For example, Equation (25) reports the velocity as function of the position. The  $\chi^2$  analysis for observed theoretical velocity as function of time/space, see **Table 2**, assigns the smaller value to the turbulent jet.

### Back reaction:

The insertion of the back reaction in the equation of motion allows us to introduce a finite rather than infinite jet's length, see Equation (39).

### The extended region:

The extended region of HH34 is modeled by combining the decreasing jet's velocity with the constant velocity and precession of the central object, see the final matrix (45).

### The theory of the image:

We have analysed the case of an optically thin layer approximation to provide an explanation for the so called "bow shock" that is visible in HH34. This effect can be reproduced when two emitting regions apparently intersect on the plane of the sky, see the numerical simulation as given by **Figure 12**. This curious effect of enhancement in the intensity of emission can easily be reproduced when the image theory is applied to the mathematical knots, see the example of the trefoil in **Figure 15**.

## Acknowledgements

Credit for **Figure 13** is given to ESO.

## Conflicts of Interest

The author declares no conflicts of interest regarding the publication of this paper.

## References

- [1] Herbig, G.H. (1950) The Spectrum of the Nebulosity Surrounding T Tauri. *The Astrophysical Journal*, **111**, 11-14. <https://doi.org/10.1086/145232>
- [2] Haro, G. (1952) Herbig's Nebulous Objects near NGC 1999. *The Astrophysical Journal*, **115**, 572-573. <https://doi.org/10.1086/145576>
- [3] Raga, A.C., Reipurth, B. and Noriega-Crespo, A. (2019) The HH34 Jet/Counterjet System at 1.5 and 4.5  $\mu\text{m}$ . *Revista Mexicana de Astronomía y Astrofísica*, **55**, 117-123. <https://doi.org/10.22201/ia.01851101p.2019.55.01.12>
- [4] Raga, A.C., Noriega-Crespo, A., Rodríguez-González, A., *et al.* (2012) The Kinematics of HH 34 from HST Images with a Nine-Year Time Baseline. *The Astrophysical Journal*, **748**, 103. <https://doi.org/10.1088/0004-637X/748/2/103>

- [5] Raga, A.C., Noriega-Crespo, A., Carey, S.J. and Arce, H.G. (2013) Proper Motions of Young Stellar Outflows in the Mid-Infrared with Spitzer (IRAC). I. The NGC 1333 Region. *Astronomical Journal*, **145**, 28. <https://doi.org/10.1088/0004-6256/145/2/28>
- [6] Noriega-Crespo, A., Raga, A.C., Moro-Martín, A., Flagey, N. and Carey, S.J. (2014) Proper Motions of Young Stellar Outflows in the Mid-Infrared with Spitzer II HH 377/Cep E. *New Journal of Physics*, **16**, Article ID: 105008. <https://doi.org/10.1088/1367-2630/16/10/105008>
- [7] Guzmán, A.E., Garay, G., Rodríguez, L.F., Contreras, Y., Dougados, C. and Cabrit, S. (2016) A Protostellar Jet Emanating from a Hypercompact H II Region. *The Astrophysical Journal*, **826**, Article No. 208. <https://doi.org/10.3847/0004-637X/826/2/208>
- [8] Raga, A.C., Reipurth, B., Esquivel, A., Castellanos-Ramírez, A., Velázquez, P.F., Hernández-Martínez, L., Rodríguez-González, A., Rechy-García, J.S., Estrella-Trujillo, D. and Bally, J. (2017) Proper Motions of the HH 1 Jet. *Revista Mexicana de Astronomía y Astrofísica*, **53**, 485-495.
- [9] Cabrit, S. and Raga, A. (2000) Theoretical Interpretation of the Apparent Deceleration in the HH 34 Super Jet. *Astronomy & Astrophysics*, **354**, 667-673.
- [10] López-Martín, L., Raga, A.C., López, J.A. and Meaburn, J. (2001) Theory and Observations of a Jet in the  $\sigma$  Orionis Region: HH 444. *Revista Mexicana de Astronomía y Astrofísica Conference Series*, **10**, 61-64.
- [11] Viti, S., Girart, J.M., Garrod, R., Williams, D.A. and Estalella, R. (2003) The Molecular Condensations Ahead of Herbig-Haro Objects. II. A Theoretical Investigation of the HH 2 Condensation. *Astronomy & Astrophysics*, **399**, 187-195. <https://doi.org/10.1051/0004-6361:20021745>
- [12] Raga, A.C., Reipurth, B., Cantó, J., Sierra-Flores, M.M. and Guzmán, M.V. (2011) An Overview of the Observational and Theoretical Studies of HH 1 and 2. *Revista Mexicana de Astronomía y Astrofísica*, **47**, 425-437.
- [13] Kwon, J., Choi, M., Pak, S., Kandori, R., Tamura, M., Nagata, T. and Sato, S. (2010) Magnetic Field Structure of the HH 1-2 Region: Near-Infrared Polarimetry of Point-Like Sources. *The Astrophysical Journal*, **708**, 758-769. <https://doi.org/10.1088/0004-637X/708/1/758>
- [14] Lee, C.F., Rao, R., Ching, T.C., Lai, S.P., Hirano, N., Ho, P.T.P. and Hwang, H.C. (2014) Magnetic Field Structure in the Flattened Envelope and Jet in the Young Protostellar System HH 211. *The Astrophysical Journal*, **797**, L9. <https://doi.org/10.1088/2041-8205/797/1/L9>
- [15] Lee, C.F., Hwang, H.C. and Li, Z.Y. (2016) Angular Momentum Loss in the Envelope-Disk Transition Region of the HH 111 Protostellar System: Evidence for Magnetic Braking? *The Astrophysical Journal*, **826**, Article No. 213. <https://doi.org/10.3847/0004-637X/826/2/213>
- [16] De Young, D.S. (2002) *The Physics of Extragalactic Radio Sources*. University of Chicago Press, Chicago.
- [17] Zaninetti, L. (2016) Classical and Relativistic Flux of Energy Conservation in Astrophysical Jets. *Journal of High Energy Physics, Gravitation and Cosmology*, **2**, 41-56. <https://doi.org/10.4236/jhepgc.2016.21005>
- [18] Zaninetti, L. (2018) Classical and Relativistic Evolution of an Extra-Galactic Jet with Back-Reaction. *Galaxies*, **27**, 134. <https://doi.org/10.3390/galaxies6040134>
- [19] Bally, J. and Devine, D. (1994) A Parsec-Scale “Superjet” and Quasi-Periodic Structure in the HH 34 Outflow? *The Astrophysical Journal*, **428**, L65. <https://doi.org/10.1086/187394>

- [20] Zaninetti, L. (2010) The Physics of Turbulent and Dynamically Unstable Herbig-Haro Jets. *Astrophysics and Space Science*, **326**, 249-262. <https://doi.org/10.1007/s10509-009-0255-8>
- [21] Goldstein, H., Poole, C. and Safko, J. (2002) Classical Mechanics. Addison-Wesley, San Francisco.
- [22] Rybicki, G. and Lightman, A. (1991) Radiative Processes in Astrophysics. Wiley-Interscience, New-York.
- [23] Hjellming, R.M. (1988) Radio Stars IN Galactic and Extragalactic Radio Astronomy. Springer-Verlag, New York. [https://doi.org/10.1007/978-1-4612-3936-9\\_9](https://doi.org/10.1007/978-1-4612-3936-9_9)
- [24] Zaninetti, L. (2009) Scaling for the Intensity of Radiation in Spherical and Aspherical Planetary Nebulae. *Monthly Notices of the Royal Astronomical Society*, **395**, 667-691. <https://doi.org/10.1111/j.1365-2966.2009.14551.x>